

Model Predictive Direct Torque Control of a Five-Level ANPC Converter Drive System

Tobias Geyer, *Senior Member, IEEE*, and Silvia Mastellone

Abstract—The five-level active neutral point clamped converter is a recently introduced topology that offers low harmonic distortion and a high output voltage. In addition to a neutral point potential in the dc-link, this topology features in each phase a flying phase capacitor. Balancing these four internal converter voltages around their references, while providing fast torque and/or current control for the machine, is an intrinsically challenging control problem. Model predictive direct torque control (MPDTC) is an ideal control methodology to address this problem. It is shown in this paper how MPDTC, originally developed for three-level inverters, can be adapted to this new five-level topology. Compared to direct torque control (DTC), the performance results of MPDTC are very promising—for the same switching frequency the harmonic distortions of the stator currents and the torque can be more than halved. At the same time the very fast torque response of DTC is maintained.

Index Terms—Model predictive control, direct torque control, model predictive direct torque control, ac motor drives, medium-voltage drives, multi-level topologies, active neutral point clamped inverter

I. INTRODUCTION

Recently, ABB introduced the active neutral point clamped (ANPC) five-level topology as the latest addition to their medium-voltage (MV) drives portfolio [1], [2]. This new drive, named ACS 2000, is available with power ratings of 1 MVA and 2 MVA, covering the low power range of the MV drives market. Using high-voltage insulated gate bipolar transistors (IGBTs), output voltages of up to 6.9 kV can be achieved. At the same time very low harmonic distortions in the stator currents result, along with acceptable dv/dt and common mode voltages. This makes the ACS 2000 particularly suitable for the retrofit market, in which direct online machines are replaced by variable speed drives. Four quadrant operation is achieved by using an active front end (AFE), which is connected via an optional transformer to the grid.

The five-level ANPC topology extends the classic three-level NPC converter [3] in two ways. The NPC diodes are replaced by active switches as in [4], and floating phase capacitors are added to each phase, similar to a flying capacitor (FC) converter [5]. This innovative topology combines the advantages of the reliable and conceptually simple NPC with the versatility of the flying capacitor converter. However, the control and modulation problem is significantly more complex than for the NPC converter. Balancing the four internal converter voltages, namely the neutral point potential and the three

phase capacitors, around their references while maintaining a low switching frequency is challenging, particularly when the phase capacitors are small [2]. At the same time, very fast control of the electrical machine quantities is to be achieved.

For the ANPC five-level topology a number of control and modulation strategies have been proposed in the literature. Virtually all of these approaches divide the control and modulation problem into two hierarchical layers. The *upper* layer controls the machine or grid currents by manipulating the three-phase converter voltages. For this, control and modulation schemes, which were originally developed for two- and three-level converters, were extended to five levels. On the machine side, this includes pulse width modulation (PWM) based on selective harmonic elimination and optimized pulse patterns [6] as well as direct torque control (DTC) [1]. On the grid side, vector control with carrier-based PWM [1], PWM based on selective harmonic elimination [7]–[10], direct power control [11] and decoupling hysteresis control [12] have been proposed. The *lower* layer maps the differential-mode voltage command of the upper layer into converter gating signals. By exploiting the redundancy in the phase voltages and switching signals, the four internal converter voltages can be balanced around their respective references. Various schemes have been reported in the literature mentioned above that aim to achieve this task.

Amongst the upper layer control techniques, DTC [13] is ABB's method of choice for their drives. DTC provides an unsurpassed fast control of the electromagnetic torque, and it is very robust with respect to parameter variations. Using hysteresis bounds on the torque and stator flux magnitude, the inverter voltage vectors are generated by a look-up table, without the use of a modulator. Model predictive direct torque control (MPDTC) significantly improves the concept of DTC, by replacing the look-up table with an online computational stage [14], [15]. MPDTC, which originates from the early 2000s, was successfully implemented and tested for an NPC inverter driving an MV induction machine, exceeding power levels of 1 MW [16]. Recently, MPDTC was generalized and further improved, by considering drastically longer prediction horizons [17]. For a broader perspective on model predictive control for power electronics and drive control problems, see [18] and some of the references therein.

Due to its ability to handle complex multi-objective drive control problem, its very fast torque response and its ability to provide very low switching frequencies and losses, MPDTC appears to be an ideal candidate to address the control and modulation problem of the ACS 2000. In particular, MPDTC

This work was done at The University of Auckland, New Zealand. T. Geyer and S. Mastellone are with ABB Corporate Research, 5405 Baden-Dättwil, Switzerland (e-mail: t.geyer@ieee.org, silvia.mastellone@ch.abb.com)

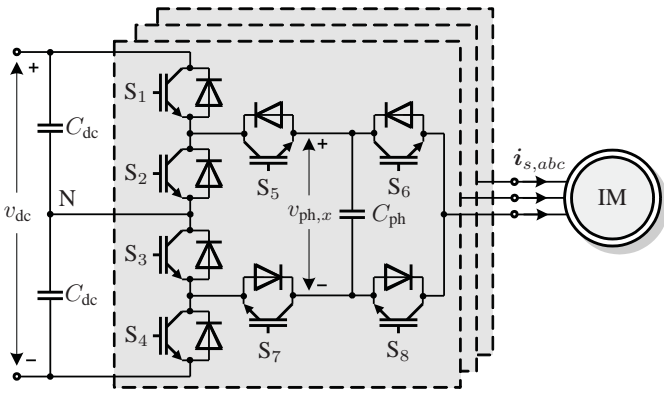


Fig. 1: Equivalent representation of the five-level active neutral point clamped (ANPC) voltage source inverter driving an induction machine (IM)

allows one to formulate and solve the control and modulation problem in one computational stage, thus addressing the torque and flux control problem as well as the balancing of the internal inverter voltages in a combined manner. As a result, the limitation inherently imposed by separating the control and modulation problem in two layers, in which the set of available solutions is inevitably cut down, is overcome. This results in a significant performance advantage. Specifically, the total harmonic distortion (THD) of the machine current can be halved, while the device switching frequency is kept unchanged, as simulations on ABB's 1MVA drive setup indicate.

In the following section we summarize the ANPC five-level topology, its switching restrictions, commutation paths and the corresponding mathematical drive model. The control problem is stated in Section III, and the MPDTC scheme is adapted and extended to the five-level topology in Section IV. In Section V the performances of MPDTC and DTC are compared, both at steady-state and during transients, showing that MPDTC achieves a reduction in the harmonic distortion levels by 50% and more for the same switching frequency, while preserving the very fast torque response of DTC. Conclusions are drawn in Section VI.

II. FIVE-LEVEL ANPC INVERTER DRIVE SYSTEM

Throughout this paper, we use normalized quantities. Extending this to the time scale t , one time unit corresponds to $1/\omega_b$ seconds, where ω_b is the base angular velocity. Additionally, we use $\xi(t)$, $t \in \mathbb{R}$, to denote continuous-time variables, and $\xi(k)$, $k \in \mathbb{N}$, to denote discrete-time variables.

All variables $\xi_{abc} = [\xi_a \ \xi_b \ \xi_c]^T$ in the three-phase system (abc) are transformed to $\xi_{\alpha\beta 0} = [\xi_\alpha \ \xi_\beta \ \xi_0]^T$ in the orthogonal $\alpha\beta 0$ stationary reference frame through $\xi_{\alpha\beta 0} = \mathbf{P} \xi_{abc}$. By aligning the α -axis with the a -axis, the following transformation matrix is obtained

$$\mathbf{P} = \frac{2}{3} \begin{bmatrix} 1 & -\frac{1}{2} & -\frac{1}{2} \\ 0 & \frac{\sqrt{3}}{2} & -\frac{\sqrt{3}}{2} \\ \frac{1}{2} & \frac{1}{2} & \frac{1}{2} \end{bmatrix}. \quad (1)$$

s_x	u_x	v_x	Switching state				Effect on	
			$S_1 S_2 S_3 S_4$	$S_5 S_6 S_7 S_8$	$v_{ph,x}$	v_n		
7	+2	$v_{dc,up}$	1 0 1 0	1 1 0 0	0	0		
6	+1	$v_{dc,up} - v_{ph,x}$	1 0 1 0	1 0 0 1	i_{sx}	0		
5	+1	$v_{ph,x}$	1 0 1 0	0 1 1 0	$-i_{sx}$	$-i_{sx}$		
4	0	0	1 0 1 0	0 0 1 1	0	$-i_{sx}$		
3	0	0	0 1 0 1	1 1 0 0	0	$-i_{sx}$		
2	-1	$-v_{ph,x}$	0 1 0 1	1 0 0 1	i_{sx}	$-i_{sx}$		
1	-1	$-v_{dc,lo} + v_{ph,x}$	0 1 0 1	0 1 1 0	$-i_{sx}$	0		
0	-2	$-v_{dc,lo}$	0 1 0 1	0 0 1 1	0	0		

TABLE I: Correspondence between the phase switch positions s_x , the phase levels u_x , the phase voltages v_x and the switching states S_1 to S_8 , for phase x , $x \in \{a, b, c\}$. The effect on the phase capacitor voltage $v_{ph,x}$ and on the neutral point potential v_n is shown on the right hand side

A. Active NPC Five-Level Inverter Topology

Consider the five-level ANPC inverter depicted in Fig. 1. The switches S_1 to S_4 consist of two series-connected IGBTs, while the switches S_5 to S_8 are single IGBTs. Thus each phase consists of 12 IGBTs. The dc-link is divided into an upper and a lower half with the two dc-link capacitors C_{dc} . The potential $v_n = 0.5(v_{dc,lo} - v_{dc,up})$ of the neutral point N floats, with $v_{dc,lo}$ and $v_{dc,up}$ denoting the voltages over the lower and the upper dc-link half, respectively. The inverter's total dc-link voltage is $v_{dc} = v_{dc,lo} + v_{dc,up}$. Neglecting the phase capacitors, this converter effectively resembles a three-level ANPC inverter with series-connected IGBTs, producing at each phase the three voltage levels $\{-\frac{v_{dc}}{2}, 0, \frac{v_{dc}}{2}\}$.

The available number of phase voltage levels is augmented to five by adding to each phase a flying capacitor C_{ph} , which is placed between the outer pairs of the existing series-connected switches S_5 to S_8 . Let the voltages across the phase capacitors be denoted by $v_{ph,x}$, with $x \in \{a, b, c\}$. The phase capacitor voltages are maintained at half the voltage levels of the individual dc-link capacitors, i.e. at $v_{ph,x} = 0.25v_{dc}$. This adds the two additional voltage levels $\{-\frac{v_{dc}}{4}, \frac{v_{dc}}{4}\}$ and ensures that each IGBT can be rated for the same voltage blocking capability. As a result, at each phase, the inverter produces the five voltage levels $\{-\frac{v_{dc}}{2}, -\frac{v_{dc}}{4}, 0, \frac{v_{dc}}{4}, \frac{v_{dc}}{2}\}$. These voltages can be described by the integer variables $u_a, u_b, u_c \in \{-2, -1, 0, 1, 2\}$, to which we refer as *phase levels*.

The phase levels $-1, 0$ and 1 can each be synthesized by two different *switch positions*, described by the integer variables $s_a, s_b, s_c \in \{0, 1, \dots, 7\}$. The phase level $u_x = 1$, for example, with $x \in \{a, b, c\}$, can be generated either with the FC switch configuration $S_5 = 1, S_6 = 0, S_7 = 0$ and $S_8 = 1$, or with $S_5 = 0, S_6 = 1, S_7 = 1$ and $S_8 = 0$. The ANPC switches are in both cases set to $S_1 = 1, S_2 = 0, S_3 = 1$ and $S_4 = 0$. As summarized in Table I, these pairs of switch positions produce effectively the same voltage at the phase terminals. This redundancy can be used to regulate the phase capacitor voltage, specifically for the pairs $s_x = 1$ and $s_x = 2$, and $s_x = 5$ and $s_x = 6$. However, these pairs affect the neutral point potential differently, adding significant complexity to the system to be handled by the control scheme.

The phase voltage is defined with respect to the dc-link mid-

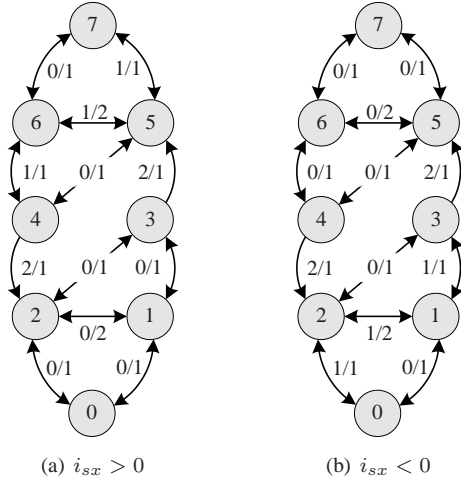


Fig. 2: Allowed per-phase switching transitions between the single-phase switch positions $s_x \in \{0, 1, \dots, 7\}$, $x \in \{a, b, c\}$, along with the number of *on* transitions of the IGBTs in the ANPC and FC part, respectively, depending on the sign of the phase current i_{sx}

point N. It is approximately $v_x = v_{dc}u_x/4$, with $x \in \{a, b, c\}$. Due to fluctuations of the dc-link and phase capacitor voltages, the precise phase voltage depends on the switch position s_x , as detailed in Table I. The three-phase voltage applied to the machine terminals is given by $\mathbf{v}_{\alpha\beta 0} = \mathbf{P} \mathbf{v}_{abc}$, with $\mathbf{v}_{\alpha\beta 0} = [v_\alpha \ v_\beta \ v_0]^T$. Neglecting the voltage fluctuations in the dc-link and the phase capacitors, the inverter produces 61 different voltage vectors, which can be synthesized by $5^3 = 125$ different phase levels $\mathbf{u} = \mathbf{u}_{abc} = [u_a \ u_b \ u_c]^T$, which in turn are established based on $8^3 = 512$ distinct switch positions $\mathbf{s} = \mathbf{s}_{abc} = [s_a \ s_b \ s_c]^T$. The 0-vector $\mathbf{v}_{\alpha\beta} = [0 \ 0]^T$, for example, can be synthesized by 26 different switch positions \mathbf{s} .

B. Switching Restrictions

A number of switching restrictions are imposed in the five-level ANPC topology, both on a single-phase as well as on a three-phase level. The allowed single-phase switching transitions are shown in Fig. 2. Switching is only possible by one voltage level up or down. Switching from $s_x = 2$ to $s_x = 4$ and from $s_x = 5$ to $s_x = 3$ is not allowed to rule out the possibility of voltage glitches. The minimum *on* time of an IGBT is $30 \mu\text{s}$. Using a sampling interval of $T_s = 25 \mu\text{s}$, this effectively leads to a minimum *on* time of $50 \mu\text{s}$.

Due to the fact that the inverter uses only two di/dt clamps—one in the upper dc-link half and another one in the lower half, restrictions on the allowed three-phase switching transitions arise. Table II summarizes the transitions that turn the clamps on and off. After a transition that turns the upper (lower) clamp on, at least $50 \mu\text{s}$ have to pass before the upper (lower) clamp may be turned off.

C. Commutation Paths

The commutation paths for this topology are rather complex. Fig. 2 summarizes the number of *on* transitions per switching

	Phase current	Transitions $s_x \rightarrow s_x$ that turn the clamp on	Transitions $s_x \rightarrow s_x$ that turn the clamp off
Upper clamp	$i_{sx} > 0$	$6 \rightarrow 4, 6 \rightarrow 5, 7 \rightarrow 5$	$4 \rightarrow 6, 5 \rightarrow 6, 5 \rightarrow 7$
	$i_{sx} < 0$	$4 \rightarrow 6, 5 \rightarrow 6, 5 \rightarrow 7$	$6 \rightarrow 4, 6 \rightarrow 5, 7 \rightarrow 5$
Lower clamp	$i_{sx} > 0$	$2 \rightarrow 0, 2 \rightarrow 1, 3 \rightarrow 1$	$0 \rightarrow 2, 1 \rightarrow 2, 1 \rightarrow 3$
	$i_{sx} < 0$	$0 \rightarrow 2, 1 \rightarrow 2, 1 \rightarrow 3$	$2 \rightarrow 0, 2 \rightarrow 1, 3 \rightarrow 1$

TABLE II: Transitions between single-phase switch positions s_x that turn a di/dt clamp on or off, depending on the sign of the phase current i_{sx} . The transitions in the upper (lower) half of the table affect the upper (lower) clamp

transition, distinguishing between the *on* transitions of the IGBTs in the ANPC and in the FC part. Switching between $s_x = 6$ and $s_x = 7$, for example, incurs no *on* transition in the ANPC part, but one in the FC part. It is clear that the number of *on* transitions always equals the number of *off* transitions. It is apparent from Table I that two *on* and two *off* transitions occur in the ANPC part when switching from $s_x = 4$ to $s_x = 2$ and from $s_x = 3$ to $s_x = 5$. On the other hand, one would expect that no IGBT is switched in the ANPC part, when the transitions occur within the group $s_x \in \{0, 1, 2, 3\}$ or $s_x \in \{4, 5, 6, 7\}$. However, in order to balance the switching load and to shift some switching losses from the FC to the ANPC part, switchings in the ANPC part do occur also in these cases, depending on the phase current. These additional ANPC switchings shift the commutation of the current from the FC to the ANPC part. From Table I it is also clear that in the FC part, for each transition, one IGBT is turned on (and another one is turned off), except for transitions occurring between $s_x = 1$ and $s_x = 2$, as well as between $s_x = 5$ and $s_x = 6$, when two devices are turned on and off.

D. Dynamics of the Internal Inverter Voltages

The evolution of the capacitor voltage in phase x , with $x \in \{a, b, c\}$, is described by the differential equation

$$\frac{dv_{\text{ph},x}}{dt} = \frac{1}{C_{\text{ph}}} \begin{cases} i_{sx}, & \text{if } s_x \in \{2, 6\} \\ -i_{sx}, & \text{if } s_x \in \{1, 5\} \\ 0, & \text{else,} \end{cases} \quad (2)$$

while the dynamic of the neutral point potential is given by

$$\frac{dv_n}{dt} = -\frac{1}{2C_{\text{dc}}} (i_{na} + i_{nb} + i_{nc}), \quad (3)$$

with i_{nx} denoting the current drawn from the neutral point

$$i_{nx} = \begin{cases} i_{sx}, & \text{if } s_x \in \{2, 3, 4, 5\} \\ 0, & \text{else.} \end{cases} \quad (4)$$

Note that the capacitor voltage of phase a , for example, only depends on the switch position and phase current of phase a , whereas the neutral point potential depends on all three switch positions and all three phase currents.

E. Induction Machine

The squirrel-cage induction motor is modelled in the $\alpha\beta$ reference frame using the α - and β -components of the stator and the rotor flux linkages per second, $\psi_{s\alpha}$, $\psi_{s\beta}$, $\psi_{r\alpha}$ and $\psi_{r\beta}$, respectively, as state variables. Neglecting the rotor speed

dynamic, the speed is effectively a model parameter rather than a state variable. The other model parameters are the base angular velocity ω_b , the stator and rotor resistances R_s and R_r , and the stator, rotor and mutual reactances L_{ls} , L_{lr} and L_m , respectively. The state equations are [19]

$$\frac{d\psi_{s\alpha}}{dt} = -R_s \frac{L_{rr}}{D} \psi_{s\alpha} + R_s \frac{L_m}{D} \psi_\alpha + v_\alpha \quad (5a)$$

$$\frac{d\psi_{s\beta}}{dt} = -R_s \frac{L_{rr}}{D} \psi_{s\beta} + R_s \frac{L_m}{D} \psi_{r\beta} + v_\beta \quad (5b)$$

$$\frac{d\psi_{r\alpha}}{dt} = R_r \frac{L_m}{D} \psi_{s\alpha} - R_r \frac{L_{ss}}{D} \psi_{r\alpha} - \omega_r \psi_{r\beta} \quad (5c)$$

$$\frac{d\psi_{r\beta}}{dt} = R_r \frac{L_m}{D} \psi_{s\beta} + \omega_r \psi_{r\alpha} - R_r \frac{L_{ss}}{D} \psi_{r\beta} \quad (5d)$$

with $L_{ss} = L_{ls} + L_m$, $L_{rr} = L_{lr} + L_m$ and $D = L_{ss}L_{rr} - L_m^2$.

The electromagnetic torque is given by

$$T_e = \frac{L_m}{D} (\psi_{s\beta} \psi_{r\alpha} - \psi_{s\alpha} \psi_{r\beta}) \quad (6)$$

and the length of the stator flux vector is

$$\Psi_s = \sqrt{\psi_{s\alpha}^2 + \psi_{s\beta}^2}. \quad (7)$$

For more details, the reader is referred to [14], [15] and [17].

III. CONTROL PROBLEM

The control problem of a high-performance variable speed drive system presents a high degree of complexity with multiple and conflicting objectives. With regards to the machine, in standard DTC and therefore also in MPDTC, the electromagnetic torque and the stator flux magnitude are to be kept within given (hysteresis) bounds and controlled dynamically with very short transients. At steady state operating conditions, the total harmonic distortion (THD) of the current is to be minimized, so as to reduce the copper losses and thus the thermal losses in the stator windings of the machine. In addition, to avoid problems with the mechanical load, such as wear of the shaft and the possible excitation of eigenfrequencies of the load, the torque THD needs to be kept at a minimum.

Since the inverter has a limited cooling capability and to ensure a safe operation of the switching devices, the total losses, particularly the switching losses, have to be kept below a given maximum value. An indirect way of achieving this is to limit the device switching frequency. The IGBTs of the FC part have to bear the majority of the switching burden. It is thus particularly important to focus on these IGBTs and to minimize their switching frequency. Additionally, the inverter's four internal voltages—the three voltages of the phase capacitors and the neutral point potential—have to be balanced around their references.

IV. CONTROL SCHEME

The machine-side controller, which is composed of cascaded control loops, is shown in Fig. 3. MPDTC constitutes the inner (torque and stator flux magnitude) control loop, which is formulated in the stationary $\alpha\beta$ reference frame. The inner loop also maintains the internal inverter voltages within given bounds. The inverter switch positions are directly set by

MPDTC, thus not requiring the use of a modulator. The inner loop is augmented in a cascaded controller fashion by outer loops, including a speed PI controller, a rotor flux controller with feedforward terms, and a loop that adjusts the bound widths for the torque and stator flux magnitude as required.

A. Model Predictive Control

Model predictive control (MPC) [20], [21] is based on five key ingredients: (i) an internal prediction model of the drive system that allows the controller to predict the effect of its control actions; (ii) a prediction horizon, which comprises a certain number of time-steps over which the controller looks into the future; (iii) a cost or objective function that represents the control objectives (e.g. the minimization of the switching frequency); (iv) an optimization stage that minimizes the cost function and yields an optimal sequence of manipulated variables (e.g. the inverter gating commands); and (v) the so called receding horizon policy. The latter implies that even though a sequence of control inputs is derived over a certain prediction horizon, only the first step is applied to the drive system. At the next time-step, new measurements and/or estimates are obtained, based on which a new, shifted sequence of manipulated variables is computed over a shifted horizon. The receding horizon policy provides feedback and robustness to the control scheme.

B. Internal Controller Model

The internal prediction model, on which MPC relies to predict the future drive trajectories, consists of three parts—the machine model, the inverter model and the inverter's switching restrictions. With regards to the machine, the standard dynamical model summarized in (5)–(7) is used. The rotor speed is assumed to be constant within the prediction horizon, which turns the speed into a time-varying parameter¹. The saturation of the machine flux and the skin effect in the rotor are neglected, even though those could be easily incorporated in the model. The dynamic model of the inverter is given in (2)–(4), which describe the dynamics of the phase capacitor voltages and of the neutral point potential. The switching restrictions are stated in Sect. II-B.

Combining the machine model (5)–(7) with the inverter model (2)–(4), and using the Euler formula, a discrete-time state-space model of the drive can be derived, which is of a similar form to the one in [15]. The system states include the stator and rotor flux vectors in $\alpha\beta$, the three phase capacitor voltages and the neutral point potential, i.e. the state vector of the drive model is $\mathbf{x} = [\psi_{s\alpha} \ \psi_{s\beta} \ \psi_{r\alpha} \ \psi_{r\beta} \ v_{ph,a} \ v_{ph,b} \ v_{ph,c} \ v_n]^T$. The switch positions \mathbf{s} constitute the input vector to the model with $\mathbf{s} \in \{0, 1, \dots, 7\}^3$. The electromagnetic torque, the stator flux magnitude, the three phase capacitor voltages and the

¹The prediction horizon being in the range of a few ms, this appears to be a mild assumption for MV drive applications. Nevertheless, for highly dynamic drives and/or drives with a small inertia, including the speed as an additional state in the model might be necessary, which is a straightforward undertaking.

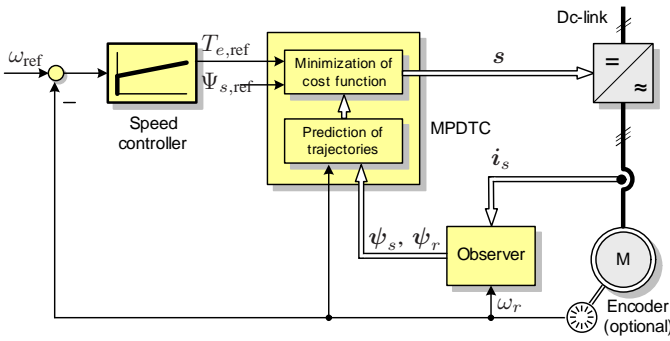


Fig. 3: Machine-side controller for the five-level active neutral point clamped (ANPC) voltage source inverter driving an induction machine. Model predictive direct torque control (MPDTC) constitutes the inner control loop

neutral point potential constitute the output vector $\mathbf{y} = [T_e \ \Psi_s \ v_{ph,a} \ v_{ph,b} \ v_{ph,c} \ v_n]^T$.

In summary, the internal prediction model includes the inverter switching behavior, restrictions on the switching transitions, the inverter dynamics and the standard dynamical model of an induction machine with four states. If required, variations on the dc-link voltage can be taken into account as well as changes of the machine's rotational speed.

C. MPDTC Control Principle and Horizons

The control objective of MPDTC is to keep the output vector within given bounds around its respective references. Specifically, the torque, stator flux magnitude, neutral point potential and the three phase capacitor voltages are to be maintained within tight bounds around their references. The inverter switch positions are directly set by MPDTC thus not requiring a modulator. The internal controller model of the drive is used to assess possible switching sequences over a long prediction horizon. The switching sequence is chosen that minimizes the predicted inverter switching frequency. Out of this sequence only the first gating signal at the current time-instant is applied. The sampling interval is typically $T_s = 25 \mu\text{s}$. Starting at the current time-step k , the MPDTC algorithm iteratively explores admissible switching sequences forward in time. At each intermediate step, all switching sequences must yield output trajectories that are either *feasible*, or *pointing in the proper direction*. We refer to these switching sequences as *candidate* sequences. *Feasibility* means that the output variable lies within its corresponding bounds; *pointing in the proper direction* refers to the case in which an output variable is not necessarily feasible, but the degree of the bounds' violation decreases at every time-step within the switching horizon. The above conditions need to hold *componentwise*, i.e. for all six output variables. Considering the effect of potential switching sequences on *all* output variables simultaneously renders the MPDTC approach particularly powerful with respect to DTC, in which switching decisions are typically based only on the *one* output variable that violates its hysteresis bound. It is important to distinguish between the switching horizon (number of switching instants within the horizon, i.e. the degrees of freedom) and the prediction horizon (number of time-steps

Induction motor	Voltage	6000 V	R_s	0.0057 pu
	Current	98.9 A	R_r	0.0045 pu
	Real power	850 kW	L_{ls}	0.0894 pu
	Apparent power	1.028 MVA	L_{lr}	0.0930 pu
	Frequency	50 Hz	L_m	2.492 pu
	Rotational speed	1494 rpm		
Inverter			v_{dc}	2.000 pu
			C_{dc}	2.201 pu
			C_{ph}	1.541 pu

TABLE III: Rated values (left) and per unit parameters (right) of the drive

MPDTC looks into the future). Between the switching instants the switch positions are frozen and the drive behavior is extrapolated until a hysteresis bound is hit. The concept of extrapolation gives rise to long prediction horizons (typically 10 to 100 time-steps), while the switching horizon is very short (usually one to three). The switching horizon is composed of the elements 'S' and 'E', which stand for 'switch' and 'extrapolate' (or more generally 'extend', respectively). We use the task 'e' to add an optional extension leg to the switching horizon. The switching horizon 'SE', for example, refers to a switching event at time-step k followed by an extrapolation segment that holds the switching position until a bound is hit. For more details about the concept of the switching horizon, the reader is referred to [17].

By varying the bound widths the resulting switching frequency, as well as the torque and current THDs can be adjusted. Specifically, by tightening the torque and flux bounds, the torque and current ripples are reduced and accordingly their THDs, while at the same time, the switching frequency is increased.

D. MPDTC Cost Function

Slightly abusing the notation, we introduce the following variables to denote the number of *on* (or *off*) transitions per phase in the ANPC and FC parts at the discrete time-step k

$$\Delta s_{\text{ANPC},x}(k) = f_{\text{ANPC}}(s_x(k-1), s_x(k)) \in \{0, 1, 2\} \quad (8a)$$

$$\Delta s_{\text{FC},x}(k) = f_{\text{FC}}(s_x(k-1), s_x(k)) \in \{0, 1, 2\}, \quad (8b)$$

where f_{ANPC} and f_{FC} are implicitly defined in Fig. 2. We also define $\Delta s_{\text{ANPC}} = \Delta s_{\text{ANPC},a} + \Delta s_{\text{ANPC},b} + \Delta s_{\text{ANPC},c}$ as the sum of the number of *on* (or *off*) transitions in all three phases. Δs_{FC} is defined accordingly.

The cost function at time-step k can then be stated as

$$c = \frac{1}{n} \sum_{\ell=k}^{k+n-1} \left(\lambda_s \Delta s_{\text{ANPC}}(\ell) + \Delta s_{\text{FC}}(\ell) \right) + \lambda_n \left(v_n(k+n-1) \right)^2 \quad (9)$$

The first part of the cost function represents the (short-term) switching frequency over the prediction horizon n . We use the tuning parameter $\lambda_s \geq 0$ to discount switchings in the ANPC part. The second part of the cost function adds a terminal weight on the neutral point potential, by penalizing the potential's deviation from zero at the end of the predicted trajectory. The penalty is adjusted using the weight $\lambda_n \geq 0$.

Control scheme	Switching horizon	Avg. prediction horizon N_p (steps)	$I_{s,\text{THD}}$ (%)	$T_{e,\text{THD}}$ (%)	$f_{\text{sw,avg}}$ (Hz)	$f_{\text{sw,ANPC}}$ (Hz)	$f_{\text{sw,FC}}$ (Hz)
DTC	—	—	100	100	421	315	634
MPDTC	'eSE'	8.4	48.6	49.9	383	272	605
MPDTC	'eSSE'	13.7	47.7	50.5	350	248	555
MPDTC	'eSESE'	19.7	47.1	49.9	337	238	534
MPDTC	'eSESESE'	30.4	45.8	48.7	326	229	519

TABLE IV: Comparison between DTC and MPDTC with various switching horizons. The comparison is done at nominal speed and full torque in terms of the current and torque THDs, $I_{s,\text{THD}}$ and $T_{e,\text{THD}}$, respectively, which are given in percentage, using DTC as a baseline, as well as the average switching frequency over all devices $f_{\text{sw,avg}}$, the switching frequency of the ANPC part $f_{\text{sw,ANPC}}$ and the switching frequency of the FC part $f_{\text{sw,FC}}$

The purpose of this second term is to reduce the likelihood of infeasibilities or deadlocks, i.e. situations in which the set of candidate switching sequences is empty. Such scenarios tend to occur, when two or more output variables are at one of their respective bounds. In most cases, the neutral point potential and one of the phase capacitor voltages act as antagonists. The likelihood of such events can be largely decreased by adding to the cost function a terminal weight on the neutral point potential. This penalty adds an incentive for MPDTC to drive the neutral point potential closer to zero, whenever the predicted increase in the switching frequency is negligible. For more details on such deadlock avoidance strategies, see [22]. In case of a deadlock, the deadlock resolution strategy outlined in [16] is employed.

E. MPDTC Control Algorithm

At time-step k , the MPDTC algorithm computes the switch position $s(k)$ according to the following procedure.

- 1) Initialize the root node with the current state vector $\mathbf{x}(k)$, the last switch position $s(k-1)$ and the switching horizon. Push the root node onto the stack.
- 2a) Take the top node with a non-empty switching horizon from the stack.
- 2b) Read out the first element. For 'S', branch on all feasible switching transitions, according to Sect. II-B and Fig. 2. Use the internal prediction model in Sect. IV-B to compute the state vector at the next time-step. For 'E', extend the trajectories either by using extrapolation, as detailed in [14], [15], or by using extrapolation with interpolation, as proposed in [23].
- 2c) Keep only the switching sequences that are candidates.
- 2d) Push these sequences onto the stack.
- 2e) Stop if there are no more nodes with non-empty switching horizons. The result of this are the predicted (candidate) switching sequences $\mathbf{S}^i(k) = [s^i(k), \dots, s^i(k+n_i-1)]$ over the variable-length prediction horizons n_i , where $i \in \mathcal{I}$ and \mathcal{I} is an index set.
- 3) Compute for each (candidate) sequence $i \in \mathcal{I}$ the associated cost c_i , as defined in (9).
- 4) Choose the switching sequence $\mathbf{S}^* = \mathbf{S}^i(k)$ with the minimal cost, where $i = \arg \min_{i \in \mathcal{I}} c_i$.
- 5) Apply (only) the first switch position $s(k) = s^*$ out of this sequence and execute the above procedure again at the next time-step $k+1$.

V. PERFORMANCE EVALUATION

In this section, for a MV five-level ANPC inverter drive system, the performance of the proposed MPDTC scheme is evaluated and benchmarked with ABB's commercial DTC scheme. For this, consider a 6 kV and 50 Hz squirrel-cage induction machine rated at 1 MVA with a total leakage inductance of $L_\sigma = 0.18$ pu. The detailed parameters of the machine and inverter are summarized in Table III. The per unit system is established using the base quantities $V_B = \sqrt{2/3}V_{\text{rat}} = 4899$ V, $I_B = \sqrt{2}I_{\text{rat}} = 139.9$ A and $f_B = f_{\text{rat}} = 50$ Hz.

For this comparison, a very accurate and detailed Matlab/Simulink model of the drive was used, which was provided by ABB to ensure as realistic a simulation set-up as possible. This model includes an observer for the motor fluxes, and various outer control loops that adjust the (time-varying) bounds on the torque and stator flux magnitude accordingly. The optional speed encoder is not used. The induction motor model includes the saturation of the machine's magnetic material and the changes of the rotor resistance due to the skin effect. Measurement and controller delays are explicitly modeled. The Simulink model includes an active front end (AFE) with a transformer and a model of the grid. The AFE regulates the total dc-link voltage and significantly affects the neutral point potential.

For MPDTC, the Simulink block with the DTC scheme is replaced by a function that runs the MPDTC algorithm at each sampling instant. The tuning parameters in the cost function are set to $\lambda_s = 0.1$ and $\lambda_n = 0.1$. The accuracy of the simulation setup and therefore the relevance of the simulation results is confirmed by the very close match between previous simulations and experimental results using a very similar Simulink model for the three-level inverter case—the simulation results in [15] predicted the experimental results in [16] accurately to within a few percent.

A. Steady-State Operation

In the following, MPDTC's performance at steady-state operating conditions is compared with the one of standard DTC. The comparison is done in terms of the current and torque THDs, $I_{s,\text{THD}}$ and $T_{e,\text{THD}}$, respectively, and the following three switching frequencies: the average of all 36 device switching frequencies, $f_{\text{sw,avg}}$; the switching frequency of the IGBT pairs S_1 to S_4 (ANPC part of the inverter), $f_{\text{sw,ANPC}}$; and the switching frequency of the IGBTs S_5 to S_8 (FC part), $f_{\text{sw,FC}}$. For MPDTC the bounds on the neutral point potential

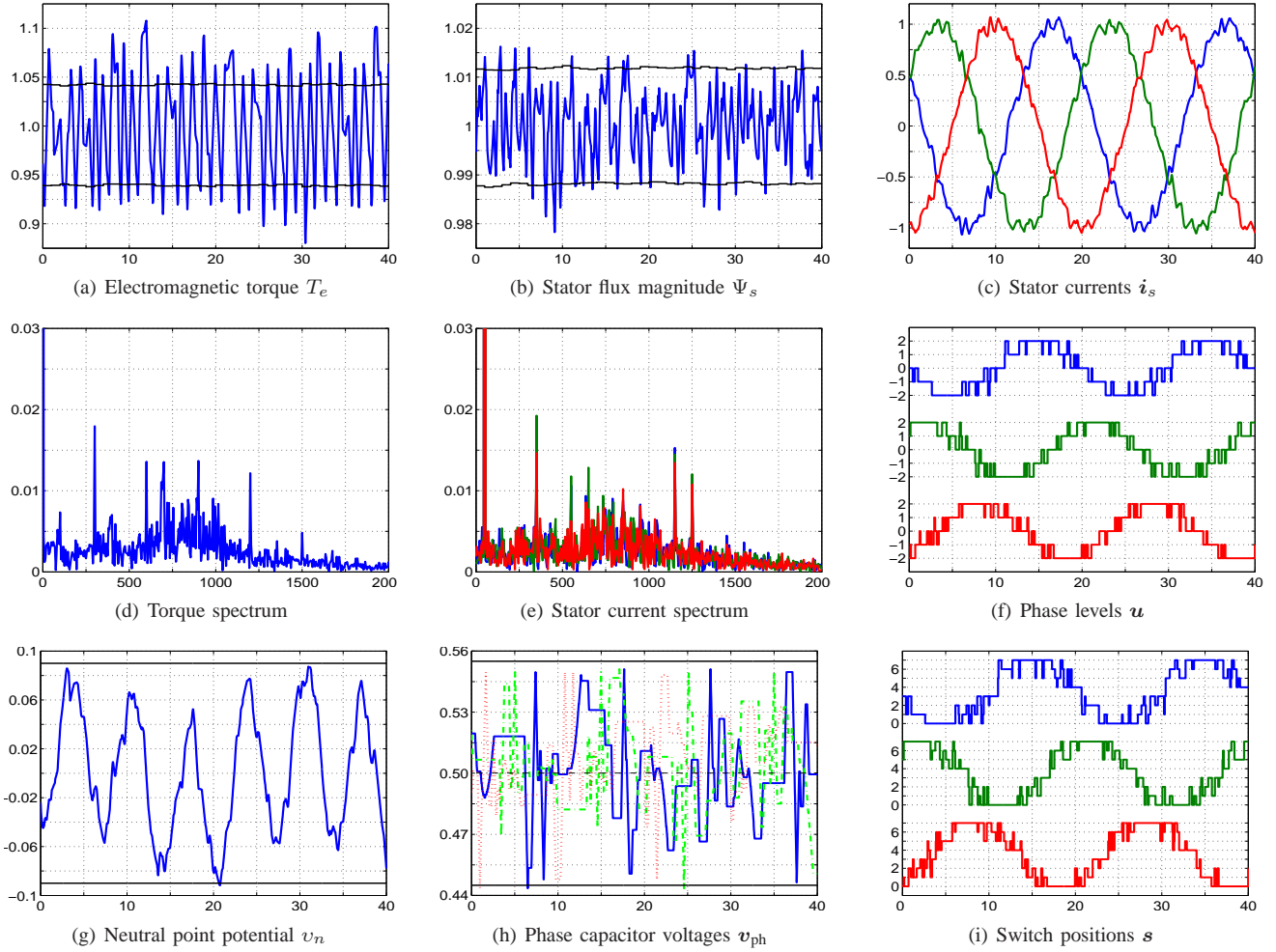


Fig. 4: Direct torque control (DTC) at rated speed and torque. The waveforms are plotted versus the time-axis in ms, except for the torque and stator current spectra, which are shown versus the frequency-axis in Hz. All quantities are given in pu

and phase capacitor voltages were kept the same as for DTC, whereas the bounds on the electromagnetic torque and stator flux magnitude were tightened. As a result and since MPDTC more closely adheres to the bounds, the current and torque THDs are more than halved for MPDTC, as summarized in Table IV.

As the switching horizon is extended, the resulting prediction horizon grows accordingly, enabling MPDTC to look further ahead and to achieve a significant reduction in the switching frequencies. For MPDTC with the switching horizon 'eSE' (i.e. one switching instant within the prediction horizon, followed by an extrapolation segment) the average switching frequency and thus the switching losses can be reduced by almost 10% with respect to DTC, whereas with the long switching horizon 'eSESESE' (i.e. three switching instants, each followed by an extrapolation segment) the average switching frequency is lowered by more than 20%. For the five-level ANPC topology the IGBTs in the FC part carry the majority of the switching burden and constitute the limiting factor. Their corresponding switching frequency can be reduced by MPDTC by 5% for 'eSE' and almost 20% for 'eSESESE'. This is a

noteworthy result, since the FC switches are predominantly used to balance the phase capacitor voltages and the controller has very little degrees of freedom to improve the balancing. Since approximately half of the switching transitions in the FC part are triggered by the internal inverter voltages, a 10% reduction enables one to tighten the bounds on the torque and stator flux by another 20% and to reduce the corresponding THDs accordingly. Interestingly, as the switching horizon is extended, the current THD also drops slightly. This indicates that the torque and stator flux are better kept within their bounds when using long prediction horizons.

Fig. 4 shows waveforms for DTC operating at nominal speed and full torque. Significant violations of the torque and stator flux bounds occur, due to the fact that DTC switches only *after* a bound has been violated. The phase currents exhibit a noticeable current ripple. The torque and current spectra were computed using the fourier transformation. The amplitudes of the harmonics are fairly small—they are below 2% of rated torque and phase current, respectively. The neutral point potential is kept well within its bounds, except for rare violations. The bounds on the phase capacitor voltages are not

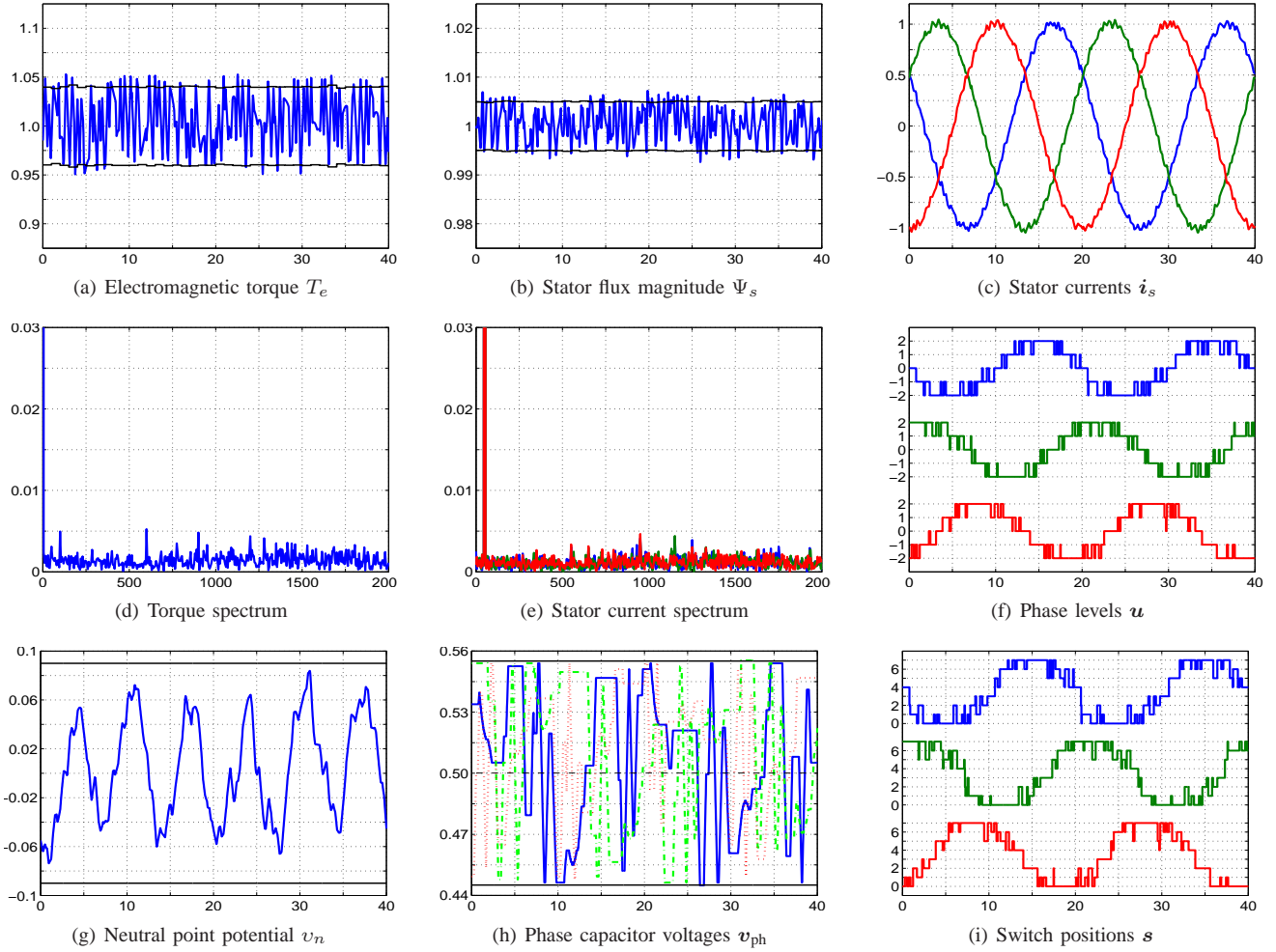


Fig. 5: Model predictive direct torque control (MPDTC) with the switching horizon 'eSESESE'. The operating point, the plots and their scalings are the same as in Fig. 4 to allow for a direct comparison. The waveforms are plotted versus the time-axis in ms, except for the torque and stator current spectra, which are shown versus the frequency-axis in Hz. All quantities are given in pu

well utilized—this is to ensure that the voltages are always kept within their bounds. To facilitate this, additional inner bounds are imposed on the phase capacitor voltages, which are not shown here. The DTC results are summarized in the first line in Table IV.

Fig. 5 shows the corresponding waveforms for MPDTC with the switching horizon 'eSESESE'. The long prediction horizon and the internal model enable MPDTC to make educated switching decisions. As a result, when compared with DTC, it was possible to significantly tighten the bounds on the torque and stator flux magnitude, while maintaining (or even slightly reducing) the switching frequency. This tightening of the bounds significantly reduces the current ripple, see Fig. 5(c), and effectively halves the current and torque THDs, as shown in Table IV. The torque and current spectra are considerably flatter and below 0.5% of rated torque and phase current, respectively. Pronounced harmonics as in DTC are avoided. The neutral point potential is kept well within its bounds, despite the unmodelled interference from the AFE. The bound width on the phase capacitor voltages is fully utilized, but not

violated, since potential violations are predicted and can thus be avoided by MPDTC.

Next, the performances of the two control and modulation schemes are compared over a range of operating points, as shown in Fig. 6. The speed is ramped up from 0.5 pu to 1.1 pu in steps of 0.05 pu, while operating at rated torque. For MPDTC the torque and stator flux bounds are scaled by the same factors as previously, whilst the bounds on the four internal inverter voltages remain unchanged. Fig. 6(a) shows the current THD achieved by MPDTC in percentage points, using DTC as a baseline. As can be seen, for this set of bounds, the current THD is halved throughout the considered range of operating points. Similarly, the torque THD, which is not shown here, is reduced by 40% to 50%.

Below 0.8 pu speed, MPDTC with the switching horizon 'eSE' greatly reduces the switching frequencies. Specifically, the average switching frequency is reduced by up to 135 Hz, whereas the switching frequency of the IGBTs in the FC part is decreased by up to 180 Hz (while simultaneously halving the current and torque THDs). It appears that MPDTC provides

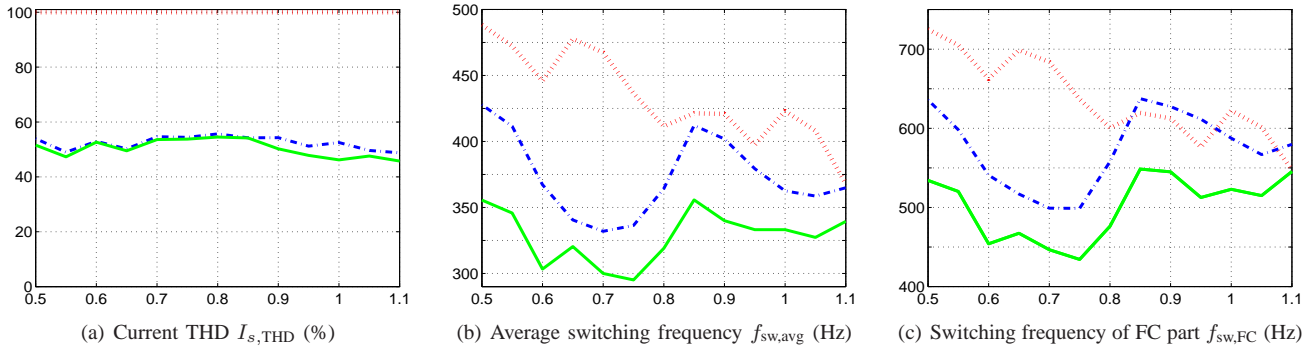


Fig. 6: Performance comparison at steady-state between MPDTC and DTC, when varying the speed setpoint ω_{ref} between 0.5 and 1.1 pu and operating at rated torque. The dashed (red) line refers to DTC, the dash-dotted (blue) line to MPDTC with the switching horizon 'eSE' and the straight (green) line refers to MPDTC with 'eSESE'

the largest performance benefit around 0.7 pu speed. A similar observation has been made for MPDTC applied to a MV drive with a NPC inverter, see [15]. For speeds above 0.8 pu, the reductions in the switching frequencies are less pronounced. Using a longer switching horizon such as 'eSESE' instead of 'eSE' reduces the average switching frequency by approximately another 45 Hz and the switching frequency of the FC devices by another 70 Hz. As can be seen from Figs. 6(b) and 6(c) the difference between the switching frequencies obtained with the switching horizons 'eSE' and 'eSESE' is pretty much independent of the speed.

B. Operation during Transients

Figs. 7 and 8 compare the performance of DTC and MPDTC with each other at nominal speed, when applying 1 pu torque steps. Both schemes are similarly fast and are effectively limited only by the voltage available and the switching restrictions. The torque settling time for negative torque steps is around 0.4 ms, while it is about 1.5 ms for positive torque steps. Overshoots in the torque occur in both schemes, which appears to be a result of the switching restrictions. All other output variables are kept well within their bounds and unnecessary switching is avoided.

It should be noted that the results shown in Fig. 8 are based on the switching horizon 'eSSE'. Shorter horizons, such as 'eSE', tend to slow down the torque response, since very short horizons in connection with the switching restrictions limit the set of voltage vectors available within the prediction horizon.

VI. CONCLUSIONS

This paper proposed a modified version of MPDTC, which was originally developed for three-level inverters, as control and modulation scheme for the recently introduced five-level ANPC topology, driving a MV induction machine with a very low total leakage inductance. The drive control and modulation problem is solved in one computational stage—unlike the approaches reported so far in the literature, which effectively all use one controller for the machine and another one for the inverter. With regards to standard DTC, the current and torque distortions can be halved, while maintaining, and in many cases reducing, the switching frequency. Model

predictive direct current control (MPDCC) [24], which is a derivative of MPDTC, might achieve a further reduction of the current THD, possibly at the expense of the torque THD, as the comparison in [25] suggests. The only major conceptual difference between the two schemes is the way the bounds are formulated. During torque transients DTC and MPDTC are both very fast.

The proposed approach is computationally demanding, requiring a powerful control platform. To facilitate the implementation, techniques from mathematical programming such as branch and bound can be used, which reduce the computation time by an order of magnitude with only a negligible impact on the performance [26]. The results presented here were obtained by implementing MPDTC on the platform used by ABB to test their drive control solutions, proving the effectiveness of MPDTC for the five-level ANPC converter drive system and its performance benefits with regards to the considerably reduced current and torque THDs. The significance of such simulations is underlined by the very close match between the previous simulation results in [15], which were obtained using a test platform similar to the one used in this paper, and the experimental results in [16].

ACKNOWLEDGMENT

The authors would like to thank Frederick Kieferndorf of ABB Corporate Research, Baden-Dättwil, Switzerland for the Matlab/Simulink files that model the ACS 2000 drive in detail. The first author gratefully acknowledges a research grant from ABB Corporate Research, Switzerland.

REFERENCES

- [1] F. Kieferndorf, M. Basler, L.A. Serpa, J.-H. Fabian, A. Coccia, and G.A. Scheuer. A new medium voltage drive system based on ANPC-5L technology. In *Proc. IEEE Int. Conf. Ind. Technol.*, pages 605–611, Viña del Mar, Chile, Mar. 2010.
- [2] P. Barbosa, P. Steimer, J. Steinke, L. Meysenc, M. Winkelkemper, and N. Celanovic. Active neutral-point-clamped multilevel converters. In *Proc. IEEE Power Electron. Spec. Conf.*, pages 2296–2301, Recife, Brasil, Jun. 2005.
- [3] A. Nabae, I. Takahashi, and H. Akagi. A new neutral-point-clamped PWM inverter. *IEEE Trans. Ind. Appl.*, IA-17(5):518–523, Sep./Oct. 1981.

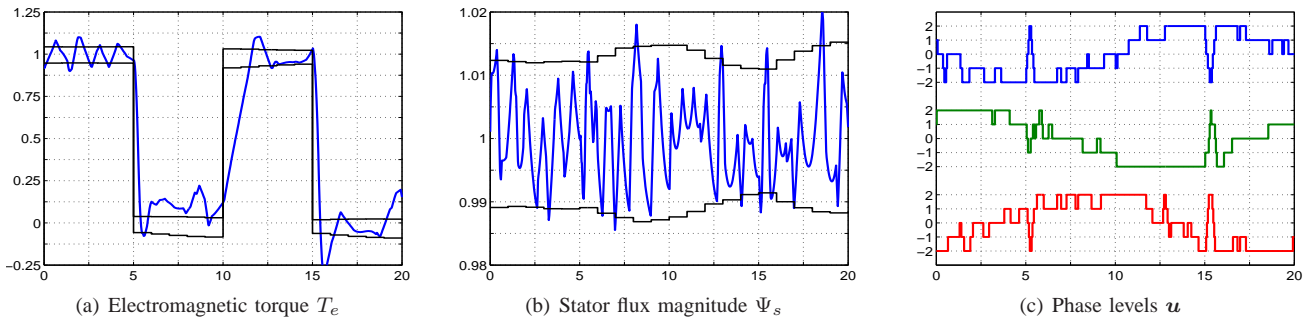


Fig. 7: Direct torque control (DTC) at rated speed and torque with nominal torque steps. The waveforms are plotted versus the time-axis in ms. All quantities are given in pu

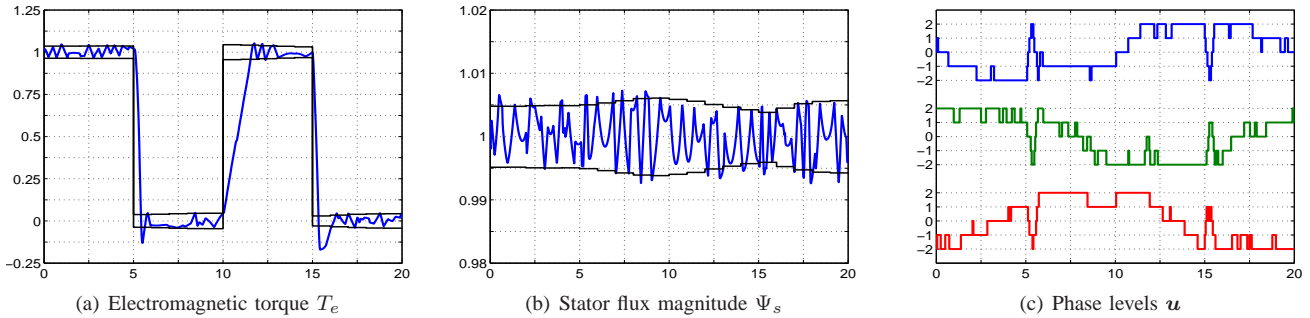


Fig. 8: Model predictive direct torque control (MPDTC) with the switching horizon 'eSSE'. The operating point, the plots and their scalings are the same as in Fig. 7 to allow for a direct comparison. The waveforms are plotted versus the time-axis in ms. All quantities are given in pu

[4] Th. Brückner, S. Bernet, and H. Guldner. The active NPC converter and its loss-balancing control. *IEEE Trans. Ind. Electron.*, 52(3):855–868, Jun. 2005.

[5] T.A. Meynard and H. Foch. Multilevel conversion: high voltage choppers and voltage source inverters. In *Proc. IEEE Power Electron. Spec. Conf.*, pages 397–403, Jun. 1992.

[6] J. Meili, S. Ponnaluri, L. Serpa, P.K. Steimer, and J.W. Kolar. Optimized pulse patterns for the 5-level ANPC converter for high speed high power applications. In *Proc. IEEE Ind. Electron.*, pages 2587–2592, 2006.

[7] S.R. Pulikanti and V.G. Agelidis. Five-level active NPC converter topology: SHE-PWM control and operation principles. In *Proc. Australasian Univ. Power Eng. Conf.*, Dec. 2007.

[8] S.R. Pulikanti, M.S.A. Dahidah, and V.G. Agelidis. SHE-PWM switching strategies for active neutral point clamped multilevel converters. In *Proc. Australasian Univ. Power Eng. Conf.*, Dec. 2008.

[9] S.R. Pulikanti and V.G. Agelidis. Control of neutral point and flying capacitor voltages in five-level SHE-PWM controlled ANPC converter. In *Proc. IEEE Conf. Ind. Electron. Appl.*, pages 172–177, 2009.

[10] S.R. Pulikanti and V.G. Agelidis. Hybrid flying capacitor based active-neutral-point-clamped five-level converter operated with SHE-PWM. *IEEE Trans. Ind. Electron.*, 58(10):4643–4653, Oct. 2011.

[11] L.A. Serpa, P.M. Barbosa, P.K. Steimer, and J.W. Kolar. Five-level virtual-flux direct power control for the active neutral-point clamped multilevel converter. In *Proc. IEEE Power Electron. Spec. Conf.*, pages 1668–1674, 2008.

[12] L.A. Serpa, P.K. Steimer, and J.W. Kolar. Virtual-flux decoupling hysteresis control for the five-level ANPC inverter connected to the grid. In *Proc. IEEE Ind. Electron.*, pages 3339–3344, Nov. 2008.

[13] I. Takahashi and T. Noguchi. A new quick response and high efficiency control strategy for the induction motor. *IEEE Trans. Ind. Appl.*, 22(2):820–827, Sep./Oct. 1986.

[14] T. Geyer. *Low Complexity Model Predictive Control in Power Electronics and Power Systems*. PhD thesis, Autom. Control Lab. ETH Zurich, 2005.

[15] T. Geyer, G. Papafotiou, and M. Morari. Model predictive direct torque control—Part I: Concept, algorithm and analysis. *IEEE Trans. Ind. Electron.*, 56(6):1894–1905, Jun. 2009.

[16] G. Papafotiou, J. Kley, K. G. Papadopoulos, P. Bohren, and M. Morari. Model predictive direct torque control—Part II: Implementation and experimental evaluation. *IEEE Trans. Ind. Electron.*, 56(6):1906–1915, Jun. 2009.

[17] T. Geyer. Generalized model predictive direct torque control: Long prediction horizons and minimization of switching losses. In *Proc. IEEE Conf. Decis. Control*, pages 6799–6804, Shanghai, China, Dec. 2009.

[18] G.C. Goodwin, D.Q. Mayne, T. Chen, C. Coates, G. Mirzaeva, and D.Q. Quevedo. Opportunities and challenges in the application of advanced control to power electronics and drives. In *Proc. IEEE Int. Conf. Ind. Technol.*, pages 27–39, Viña del Mar, Chile, Mar. 2010.

[19] P. C. Krause, O. Wasynczuk, and S. D. Sudhoff. *Analysis of Electric Machinery and Drive Systems*. Intersci. Publ. John Wiley & Sons Inc., 2nd edition, 2002.

[20] C. E. Garcia, D. M. Prett, and M. Morari. Model predictive control: Theory and practice—A survey. *Automatica*, 25(3):335–348, Mar. 1989.

[21] J. B. Rawlings and D. Q. Mayne. *Model predictive control: Theory and design*. Nob Hill Publ., Madison, WI, USA, 2009.

[22] Th. Burtcher. Deadlock avoidance and resolution for model predictive direct torque control. Master's thesis, ETH Zurich, May 2011.

[23] Y. Zeinaly, T. Geyer, and B. Egardt. Trajectory extension methods for model predictive direct torque control. In *Proc. App. Power Electron. Conf. and Expo.*, pages 1667–1674, Fort Worth, TX, USA, Mar. 2011.

[24] T. Geyer. Model predictive direct current control: formulation of the stator current bounds and the concept of the switching horizon. *IEEE Ind. Appl. Mag.*, 18(2):47–59, Mar./Apr. 2012.

[25] T. Geyer. A comparison of control and modulation schemes for medium-voltage drives: emerging predictive control concepts versus PWM-based schemes. *IEEE Trans. Ind. Appl.*, 47(3):1380–1389, May/Jun. 2011.

[26] T. Geyer. Computationally efficient model predictive direct torque control. *IEEE Trans. Power Electron.*, 26(10):2804–2816, Oct. 2011.